PHYSICAL REVIEW B **82**, 165448 (2010)

Nitrogen-induced roughening of Re surfaces on the atomic scale

Payam Kaghazchi and Timo Jacob*
Institut für Elektrochemie, Universität Ulm, Albert-Einstein-Allee 47, D-89069 Ulm, Germany
(Received 12 September 2010; published 28 October 2010)

Using density-functional theory (DFT) in combination with thermodynamic considerations the morphology change in Re($11\bar{2}1$) in the presence of a nitrogen atmosphere has been investigated. In agreement with experimental observations, we find that nitrogen adsorption causes two-sided ridges consisting of atomically rough Re($13\bar{4}2$) and ($31\bar{4}2$) faces to become much more favorable than the initially planar Re($11\bar{2}1$). We show that this surface faceting is due to a strong preference of N to adsorb at specific surface sites on Re($13\bar{4}2$). Our studies suggest that it is possible to stabilize atomically rough surfaces with high density of steps and kinks by the adsorption of certain strongly interacting adsorbates.

DOI: 10.1103/PhysRevB.82.165448 PACS number(s): 68.03.−g, 71.20.Be, 71.15.Mb

I. INTRODUCTION

Atomically rough, high-index surfaces generally show better performance as catalysts than their close-packed counterparts,[1] which is usually caused by the high density of low-coordinated surface sites being rather active for many reactions. For instance, it has been shown that Ir(210) is very active for NO decomposition with high selectivity to N_2.[2] Similarly, Pt(210) was found to have high catalytic activity for the electroreduction of CO_2,[3] and unusually high activity for NO decomposition has been evidenced on Pt(410).[4] Further, a one-dimensional oxide structure that formed at steps of the Pt(332) surface (after O_2 exposure) was found to be highly active for CO oxidation.[5]

Since recent years Re [hexagonally close-packed (hcp)] and Re-based catalysts have been used in many important catalytic reactions such as the selective reduction in NO_x with NH_3, the selective oxidation of methanol, thiophene and hydrodesulfurization, or the ammonia synthesis.[6–11] Nevertheless, only few studies have been devoted to the investigation of Re surfaces in the presence of simple reactants such as nitrogen, oxygen, and hydrogen.[12–17]

Open surfaces with low-coordinated atoms are unlikely to remain stable during catalytic reactions. In the presence of strongly interacting adsorbates, atomically rough surfaces often become morphologically unstable. For instance, in the following transformations, initially planar surfaces break up to form nanofacets of more close-packed orientations when covered with O and annealed at elevated temperatures: planar Rh(553)→{331} and {111} facets,[18] planar Pd(553)→{332} facets,[19] planar W(111)→{112} facets, planar Mo(111)→{112} facets, planar Ir(210)→{110} and {311} facets, and planar Re($11\bar{2}1$)→{$10\bar{1}0$} and {$10\bar{1}1$} facets.[20] Since rough surfaces often show higher chemical activity in comparison to their close-packed counterparts, facets consisting of open surfaces can be promising candidates for various catalytic applications.

Recently, Wang *et al.* have shown that in the presence of nitrogen initially planar Re($11\bar{2}1$) becomes completely faceted at 900 K and a pressure of 5×10^{-10} atm. In their experiments nitrogen was introduced by exposing the system to ammonia at temperatures above 600 K, where it decomposes to leave only N atoms on the surface. The facets that appeared were characterized as ridgelike structures with faces having ($13\bar{4}2$) and ($31\bar{4}2$) orientations.[17] Interestingly, these rough surfaces, which form on the facets upon nitrogen adsorption, are considerably more stable than initial Re($11\bar{2}1$), which is even more close packed. This behavior is different compared to many other systems, where after surface faceting more close-packed faces are exposed.

Motivated by these experiments, the present work aims at an atomistic understanding of the experimentally observed ridgelike structures that form on the planar Re($11\bar{2}1$) substrate after nitrogen adsorption. For this purpose, the relevant clean and N-covered surfaces are investigated by means of density-functional theory (DFT) calculations, providing the most stable structures, binding energies, diffusion barriers, and density of states. Using the obtained energies in conjunction with the *ab initio* atomistic thermodynamics approach,[21–24] we generate a phase diagram for surface faceting, which is readily comparable to the experimental observations.

The paper is organized as follows. Section II briefly describes the DFT calculations, the *ab initio* atomistic thermodynamics method, and conditions under which facet formation should occur. Our DFT results for Re bulk as well as for the clean and nitrogen-covered surfaces of planar Re($11\bar{2}1$) and Re($13\bar{4}2$) facets are described in Sec. III. This information allows us to construct the corresponding faceting phase diagram (Sec. IV). Finally, conclusions will be given in Sec. V.

II. METHOD

The macroscopic behavior of materials is mostly determined by the interactions at the microscopic level. Therefore, in order to investigate the adsorbate-induced surface faceting, we first employed DFT to obtain information on surface adsorption and binding energies (microscopic scale), which were then used in conjunction with statistical mechanics to bridge toward the macroscopic behavior. In particular, the *ab initio* atomistic thermodynamics approach had been used to evaluate (p,T)-dependent surface free energies,[21–24] which

together with the facet formation condition allowed us to draw conclusions on the surface faceting.

A. DFT calculations

All first-principles calculations were performed with the Cambridge serial total energy package (CASTEP),[25] a periodic plane-wave-based DFT program. We have used Vanderbilt-type ultrasoft pseudopotentials[26] to replace the core electrons while the valence space had been expanded in plane waves up to an energy cutoff of 380 eV, which in extensive convergence tests was found to be appropriate for the present system.[27,28] Throughout this work, exchange-correlation (xc) energies were evaluated with the Perdew-Burke-Ernzerhof (PBE) (Ref. 29) form of the generalized-gradient approximation. However, in order to evaluate the influences related to the density functional, some of the key systems were additionally calculated with the local-density approximation (LDA) functional for comparison.

Adsorption of nitrogen on Re(11$\bar{2}$1) and (13$\bar{4}$2), which are the surface orientations relevant for the faceting, had been studied at various surface sites, coverages, and adlayer configurations. While Re(11$\bar{2}$1) had been represented by a 19-layer slab, the more open Re(13$\bar{4}$2) required 30-layer slabs to ensure for layer-converged binding energies. All slab geometries were generated on the basis of the calculated lattice constants of a_0=2.78 Å and c_0=4.48 Å,[27] with periodic slab images separated by at least 13 Å vacuum. For Re(11$\bar{2}$1) the bottom four and for Re(13$\bar{4}$2) the bottom 14 layers were fixed at the calculated bulk structure while all remaining layers plus adsorbates were fully optimized (up to $<$0.03 eV/Å) using the Broyden-Fletcher-Goldfarb-Shanno method[30] as implemented in CASTEP. Finally, for integrations in reciprocal-space Brillouin zones of the (1×1) surface unit cells of Re(11$\bar{2}$1) and (13$\bar{4}$2) were sampled with (4×4) and (3×3) Monkhorst-Pack **k**-point meshes, respectively.

B. *Ab initio* atomistic thermodynamics approach

We assume that a surface is in thermodynamic equilibrium with different phases (e.g., a macroscopic bulk phase and/or a surrounding gas phase environment) that can give (or take) any amount of atoms to (or from) the surface without changing the temperature or pressure. The appropriate thermodynamic potential for such a system is the Gibbs energy,

$$G = U - TS + pV, \tag{1}$$

where U is the internal energy and S the entropy. The most stable surface structure under given temperature and pressure conditions is the one that has the lowest surface free energy, which can be written as

$$\gamma(T,\{p_i\},\{N_i\}) = \frac{1}{A}\left[G_{\text{surf}}(T,\{p_i\},\{N_i\}) - \sum_i N_i\mu_i(T,p_i)\right] \quad \text{with } (i=\text{Re,N}), \tag{2}$$

where G_{surf} is the Gibbs energy of a particular surface with the area A, which consists of N_i atoms of the ith species whose reservoir is characterized by the chemical potential $\mu_i(T,p_i)$. Due to the minor temperature and pressure dependence of the Re-bulk reservoir, its chemical potential can be approximated by the Gibbs energy (or corresponding bulk cohesive energy). By assuming ideal behavior for the surrounding gaseous reservoirs, μ_{gas} can be related to specific temperatures and pressures. For instance, for a N_2 atmosphere we can write

$$\mu_{\text{N}}^{\text{gas}}(T,p_{\text{N}_2}) = \frac{1}{2}\left[E_{\text{N}_2}^{\text{tot}} + \bar{\mu}_{\text{N}_2}(T,p^0) + k_{\text{B}}T\ln\left(\frac{p_{\text{N}_2}}{p^0}\right)\right]. \tag{3}$$

Here, $E_{\text{N}_2}^{\text{tot}}$ is the calculated total energy of an isolated N_2 molecule and $\bar{\mu}_{\text{N}_2}(T,p^0)$ is the standard chemical potential at temperature T, which includes all the contributions from vibrations and rotations of the molecule, and the ideal gas entropy at 1 atm. Although the standard chemical potentials can be calculated from first principles, for the phase diagram, which will be discussed later, we used the corresponding $\bar{\mu}_{\text{N}_2}(T,p^0)$ values from the JANAF thermodynamic tables.[31]

For solid phases the Gibbs energy, defined by Eq. (1), can be written as

$$G = E_{\text{tot}} + F_{\text{conf}} + F_{\text{vib}} + pV, \tag{4}$$

where E_{tot} is the total energy, F_{conf} the configurational free energy, and F_{vib} the vibrational free energy. The largest contribution to Eq. (4) arises from the first term E_{tot}, which in the present work is obtained by DFT calculations. An exact evaluation of F_{conf} needs large computational effort since various adlayer configurations have to be studied for each coverage. Fortunately, for sufficiently low temperatures this term is usually much smaller than the total energy term in Eq. (4) and can therefore be neglected. The vibrational free energy contains the zero-point energy E^{ZPE} and the entropy contribution S^{vib}. For our case of N adsorbed on a Re surface this leads to

$$F^{\text{vib}}(T,V,N_{\text{Re}},N_{\text{N}}) = \int d\omega F^{\text{vib}}(T,\omega)\sigma(\omega) = E^{\text{ZPE}} - TS^{\text{vib}}, \tag{5}$$

where $\sigma(\omega)$ is the phonon density of state (DOS) and the frequency-dependent function $F^{\text{vib}}(T,\omega)$ is

$$F^{\text{vib}}(T,\omega) = \frac{1}{2}\hbar\omega + k_{\text{B}}T\ln(1-e^{-\hbar\omega/k_{\text{B}}T}). \tag{6}$$

The vibrational contribution to the surface free energy, γ^{vib}, is then obtained as the difference of the vibrational energy of atoms on the surface and in the reservoirs,

$$\gamma^{\text{vib}}(T,V) = \frac{1}{A}\int F^{\text{vib}}(T,\omega)\left[\sigma_{\text{surf}}(\omega) - N_{\text{Re}}\sigma_{\text{Re}}^{\text{bulk}}(\omega) - \frac{N_{\text{N}}}{2}\sigma_{\text{N}_2}^{\text{gas}}(\omega)\right]d\omega. \tag{7}$$

Although the entire phonon DOS of the surfaces can be obtained by DFT, in the present work we use the Einstein model in which the phonon DOS is simply a delta function at

one characteristic frequency $\bar{\omega}$. If we assume that the vibrational frequency of the metal atoms of the clean surface is similar to that after N adsorption, then the vibrational contributions to γ coming from nitrogen can be estimated by

$$\gamma^{\mathrm{vib}}(T) \sim \frac{1}{A}\left[\sum_{i}^{N_{\mathrm{N}}} F_i^{\mathrm{vib}}(T,\bar{\omega}_i^{\mathrm{surf}}) - \frac{N_{\mathrm{N}}}{2}F^{\mathrm{vib}}(T,\bar{\omega}_{\mathrm{N}_2}^{\mathrm{gas}})\right], \quad (8)$$

where $\bar{\omega}_i^{\mathrm{surf}}$ is the N-surface stretch frequency of the ith adsorbed nitrogen in the corresponding configuration and $\bar{\omega}_{\mathrm{N}_2}^{\mathrm{gas}}$ is for the N_2 molecule in the gas phase. Using this approach the vibrational contributions to γ were estimated for the most stable configurations determined in our calculations. In all cases, we found that these contributions are rather small and they cause no modifications in the ordering of surface phases. Therefore, in the final surface phase diagram vibrational contributions have not been included.

From a dimensional analysis it can easily be seen that the last term of Eq. (4), the pV term, will be less than ~ 0.001 meV/Å^2 for pressures up to 1 atm and can therefore be neglected, too. Finally, we come to the conclusion that the temperature and pressure dependence of the solid phases (surface and bulk) is expected to be much smaller than that of gaseous phases, whose chemical potentials dominate the T and p dependence of the surface free energies. Therefore, the difference in the Gibbs energy of the slab and the bulk can be replaced by their corresponding total energies, which then can be evaluated by DFT calculations (see Sec. II A).

C. Considerations on the formation of facets

Herring has made important contributions to the theory of the thermodynamic stability of crystal surfaces.[32] One of the important conclusion of Herring's work was: "if a given macroscopic surface of a crystal does not coincide in orientation with some portion of the boundary of the equilibrium shape, there will always exist a hill-and-valley structure, which has a lower free energy than a flat surface, while if the given surface does occur in the equilibrium shape, no hill-and-valley structure can be more stable." Therefore, one would expect that under certain conditions a flat surface minimizes the overall stability, γ, by converting to a "hill-and-valley" structure, exposing new crystal faces.

Since facet formation is thermodynamically driven, the important quantity is the formation energy, which can be expressed as a sum of changes in the Gibbs energies, which is mainly related to surface, edge, corner, and strain contributions,

$$\Delta G^{\mathrm{form}} = \Delta G^{\mathrm{surface}} + \Delta G^{\mathrm{edge}} + \Delta G^{\mathrm{corner}} + \Delta G^{\mathrm{strain}} + \cdots . \quad (9)$$

Assuming the facets to be large, the overall formation energy can be approximated by the surface contribution only. On the basis of this assumption and with the definition of Eq. (9), facet formation should occur if

$$\Delta G^{\mathrm{form}} \approx \Delta G^{\mathrm{surface}} = \sum_f A_f^{\mathrm{final}}\gamma_f^{\mathrm{final}} - A^{\mathrm{initial}}\gamma^{\mathrm{initial}} < 0, \quad (10)$$

where the initial surface is characterized by the surface free energy $\gamma^{\mathrm{initial}}$ and an overall surface area A^{initial}, and the fth face of the facets accordingly by γ^{final} and A^{final}. Since in the present case, two-sided ridges consisting of Re(13$\bar{4}$2) and (31$\bar{4}$2) facets are formed on the initially planar Re(11$\bar{2}$1) surface after adsorption of nitrogen, Eq. (10) converts into the following condition, which has to be fulfilled in order to show facet formation

$$\frac{S_{13\bar{4}2}}{\cos\vartheta_{13\bar{4}2}}\cdot\gamma_{13\bar{4}2}(T,p_{\mathrm{N}_2}) + \frac{S_{31\bar{4}2}}{\cos\vartheta_{31\bar{4}2}}\cdot\gamma_{31\bar{4}2}(T,p_{\mathrm{N}_2}) - \gamma_{11\bar{2}1}(T,p_{\mathrm{N}_2}) < 0. \quad (11)$$

Here, S specifies the partial contribution of the different faces to each nanoshaped facet, while ϑ is the tilt angle of the faces with respect to the initial substrate, T the temperature, and p_{N_2} the partial pressure of the surrounding nitrogen gas, whose adsorption induces the faceting. While all previously mentioned parameters are either given by the experimental conditions (i.e., T and p_{N_2}) or can be obtained by geometrical considerations (i.e., S and ϑ), the remaining information required for Eq. (11) are the surface free energies of the initial substrate, as well as the faces of the final facets. To evaluate the different surface free energies relevant to Eq. (11), the above-mentioned *ab initio* atomistic thermodynamics approach can be used, which allows for evaluating the stability of surfaces/interfaces that are in contact and in thermodynamic equilibrium with a surrounding atmosphere.

III. RESULTS AND DISCUSSION

A. Bulk rhenium

After extensive convergence tests, we determined that a Monkhorst-Pack **k**-point mesh of $(8\times8\times5)$ and an plane-wave energy cut-off value (380 eV) led to converged results for Re bulk.[28] The obtained lattice constants, bulk modulus, and cohesive energy that were obtained using the PBE and LDA functionals are summarized in Table I.

Our pseudopotential results (USPP) were found to be in good agreement with corresponding all-electron (AE) calculations. Although both PBE and LDA yielded satisfactory results for lattice constants, the PBE bulk modulus and cohesive energy were expectedly closer to the experimental values. Hence, for the present studies we used mainly the PBE functional and recalculate the stability of the most stable structures by LDA.

Figure 1 shows the calculated projected DOS (PDOS) of Re bulk expressed as

$$D_\alpha(\epsilon) = \sum_{i=1}^{\infty} |\langle\varphi_\alpha|\phi_i\rangle|^2\delta(\epsilon-\epsilon_i), \quad (12)$$

where φ_α is the function onto which the DOS is projected on. In the present case ϕ_i and ϵ_i are the Kohn-Sham orbitals and eigenvalues.

TABLE I. Calculated lattice parameters (a_0 and c_0), bulk modulus (B_0), and cohesive energy (E_{coh}) of bulk Re, determined with USPP and AE approaches using the PBE and LDA exchange-correlation functionals. In addition, the experimental values are given.

Method	a_0 (Å)	c_0 (Å)	B_0 (Mbar)	E_{coh} (eV)
USPP (PBE)	2.78	4.48	3.65	−7.63
USPP (LDA)	2.73	4.41	4.05	−9.45
AE (PBE)	2.78	4.48	3.63	−7.70
AE (LDA)	2.74	4.42	4.06	−9.59
Expt.[a]	2.76[b]	4.46[b]	3.72[b]	−8.03[c]

[a]Reference 33.
[b]At room temperature.
[c]At 0 K and 1 atm.

From the PDOS plot of Re bulk, the following information can be extracted: (1) the *d* band has considerably larger contributions to the total valence DOS compared to *s* and *p* orbitals; (2) the *d* band is narrower (more localized) than the *s* and *p* bands; and (3) the integral of the *d* band up to the Fermi energy is almost equal to that above the Fermi energy, which reflects the fact that rhenium has a half-filled *d* band.

B. Clean Re surfaces

The hcp structures, such as adopted by metallic rhenium, involve two interpenetrating Bravais lattices. In this kind of material, we have two classes of atoms, which are distinguishable in their environment. Therefore, in most cases cleaving the hcp crystal along a particular direction creates two different surface structures depending on which kind of atoms are exposed (by displacing the dividing plane). Using the four-index notation we label the different possible terminations of Re surfaces by (*ijkl*)A and (*ijkl*)B.

1. Re(11$\bar{2}$1)

Figure 2 shows that Re(11$\bar{2}$1)A and Re(11$\bar{2}$1)B are mirror symmetric of each other and have the same surface termination. Our DFT-PBE calculations reproduce this fact, showing a surface free energy of 220 meV/Å^2 for both

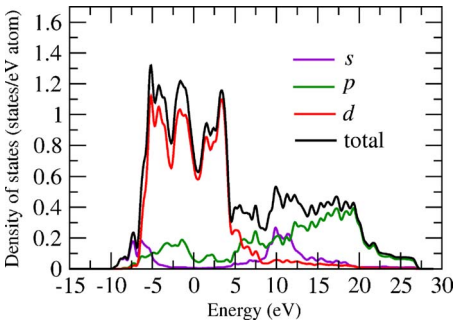

FIG. 1. (Color online) Partial density of states (projected onto *s*, *p*, and *d* orbitals) and total density of states for rhenium bulk. The energy zero corresponds to the Fermi level.

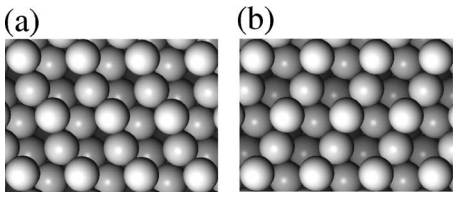

FIG. 2. Top views of (a) Re(11$\bar{2}$1)A and (b) Re(11$\bar{2}$1)B. The layers become darker with increasing depth.

Re(11$\bar{2}$1)A and Re(11$\bar{2}$1)B. Therefore, here we continue our studies by considering one of these configurations [Re(11$\bar{2}$1)A] and for simplicity refer to it as Re(11$\bar{2}$1). This is also justified by the fact that both A and B structures are equivalent in the sense that they have the same nearest- and next-nearest-neighbor structures and distances.

As expected, the calculated surface free energy for Re(11$\bar{2}$1) is larger using the LDA functional than with PBE (see Table II). Regarding the surface relaxation, our PBE calculations show that the outermost layers are strongly contracted (Δd_{12}=−14.8%, Δd_{23}=−20.6%, and Δd_{34}=−15.7%) compared to the bulk layer spacings of d_{ij}^{bulk}=0.663 Å. These contractions are compensated by a very large expansion in the fourth interlayer separation (28.4%). The strong relaxations are certainly related to the high cohesive energy of Re. Although there are no experimental or theoretical data on this surface to compare our values with, experimental studies on Re(10$\bar{1}$0) have also shown a large inward relaxation of the first surface layer of ~17%.[34,35]

2. Re(13$\bar{4}$2)/Re(31$\bar{4}$2)

Both terminations of Re(13$\bar{4}$2) are very open and have eight layers of atoms exposed (see Fig. 3). We found that with the PBE functional both configurations have the same surface free energy of 217 meV/Å^2. Interestingly, this value is only 3 meV/Å^2 lower than that obtained for Re(11$\bar{2}$1). The Re(13$\bar{4}$2) surface is much more open than Re(11$\bar{2}$1) and one might expect the former structure to be much less stable. This behavior is probably due to the unique structure of Re(13$\bar{4}$2), which is vicinal to the (01$\bar{1}$1) orientation with kinked steps and (01$\bar{1}$1) terraces that are more close-packed than (11$\bar{2}$1).[17] This is also supported by the fact that clean

TABLE II. Surface free energies (in meV/Å^2) for Re surfaces as well as two-sided ridges of (13$\bar{4}$2) and (31$\bar{4}$2) obtained using the PBE and LDA functional.

Structure	PBE	LDA
Re(11$\bar{2}$1)A	220	255
Re(11$\bar{2}$1)B	220	
Re(13$\bar{4}$2)A	217	251
Re(13$\bar{4}$2)B	217	
Two-sided ridges	225	261

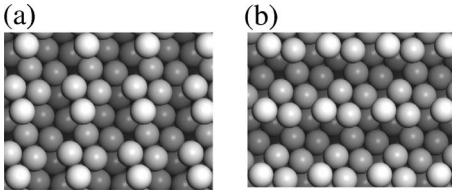

FIG. 3. Top views of (a) Re(13$\bar{4}$2)A and (b) Re(13$\bar{4}$2)B. The layers become darker with increasing depth.

Re(13$\bar{4}$2) is only 4 meV/Å^2 less stable than low-index Re(01$\bar{1}$1),[28] which means that the presence of kinks and steps reduces the stability of Re(13$\bar{4}$2) compared to Re(01$\bar{1}$1), although their contributions to the surface free energy of Re(13$\bar{4}$2) are insignificant. As we will see in Sec. III D 2, adsorption of nitrogen at a site between Re(01$\bar{1}$1) terraces causes Re(13$\bar{4}$2) to become energetically much more stable than Re(11$\bar{2}$1).

Because of the similar stability of Re(13$\bar{4}$2)A and B, again we focus on one of these configurations [Re(13$\bar{4}$2)A], and refer to it as Re(13$\bar{4}$2). Similar to the case of Re(11$\bar{2}$1), LDA yields larger surface free energies for Re(13$\bar{4}$2) compared to PBE. The changes in the interlayer spacings of clean Re(13$\bar{4}$2)A (calculated with PBE) are $\Delta d_{12}=-31.2\%$, $\Delta d_{23}=-4.4\%$, $\Delta d_{34}=-35.6\%$, and $\Delta d_{45}=13.2\%$ with respect to the corresponding bulk distances of $d_{12}^{\text{bulk}}=d_{34}^{\text{bulk}}=0.426$ Å and $d_{23}^{\text{bulk}}=d_{45}^{\text{bulk}}=0.213$ Å.

3. *Density of states of clean* Re(11$\bar{2}$1) *and* Re(13$\bar{4}$2)

In Sec. III A we have seen that the DOS of Re bulk is dominated by its *d* states. In Fig. 4 we show the density of states (projected onto the *d* orbitals) of the uppermost surface layers of Re(11$\bar{2}$1) and Re(13$\bar{4}$2) as calculated with the PBE functional. According to a simple tight-binding model, the bandwidth should decrease with decreasing coordination of the surface atoms. Therefore, as can be seen in Fig. 4, for both surfaces the *d* band of the topmost surface atoms is narrower compared to that of the bulk atoms.

Due to the increase in coordination number, the *d* bands of lower-lying atoms become wider and more comparable to bulk atoms. Although for Re(11$\bar{2}$1) the fifth-layer atoms resemble almost bulk behavior, for Re(13$\bar{4}$2) the sixth layer still has a narrowed *d* band. This is clearly due to the fact that the latter surface is more open and even its sixth layer is exposed, meaning these atoms are still lower coordinated than an atom in Re bulk.

C. Clean Re facets

Without N adsorption, the Re(13$\bar{4}$2) facets that have been observed experimentally on Re(11$\bar{2}$1) after N adsorption would be thermodynamically stable if the surface free energies of the planar and the faceted surface would meet the condition given in Eq. (11). Using the facet tilt angles (ϑ)

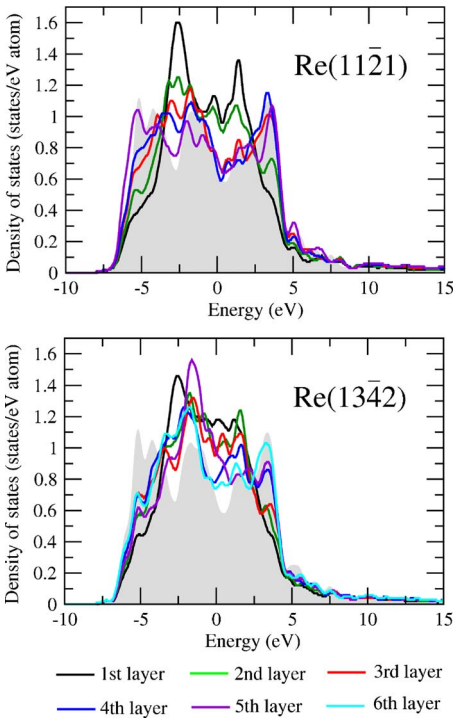

FIG. 4. (Color online) Partial density of states projected onto the *d* orbitals for different Re surfaces. The gray shaded areas correspond to the *d* states of Re bulk. The energy zero was referenced to the Fermi level.

and partial surface contributions summarized in Table III, we evaluated the overall γ of two-sided ridges combining (13$\bar{4}$2) and (31$\bar{4}$2) faces (see Table II).

Although our calculations showed that Re(13$\bar{4}$2) is slightly more stable than Re(11$\bar{2}$1), the overall surface free energy of two-sided ridgelike (13$\bar{4}$2) facets, calculated by the left side of Eq. (11), is 5 meV/Å^2 less stable than planar Re(11$\bar{2}$1). Here we have neglected edge and kink contributions to the surface energies since the experimentally observed facets were characterized to be rather extended. Including these contributions would even further reduce the overall stability of two-sided ridgelike structures. Even when using the LDA functional, the two-sided ridgelike structures turned out to be less favorable than the planar Re(11$\bar{2}$1) surface (by 6 meV/Å^2). Therefore, in agreement with the experiment, we find that without N adsorption no faceting should occur.

TABLE III. Surface area *A* [per 1×1 unit cell (calculated)], partial surface contributions (*S*), and tilt angles (ϑ) for the initial substrate and two-sided ridges consisting of (13$\bar{4}$2) and (31$\bar{4}$2) faces. For *S* the experimentally measured and geometrically derived values are given (Ref. 17).

Surface	*A* (Å^2)	S^{exp}	S^{geo}	ϑ^{geo} (deg)
Re(11$\bar{2}$1)	22.54			
Re(13$\bar{4}$2)/(31$\bar{4}$2)	46.77	0.5	0.5	15.42

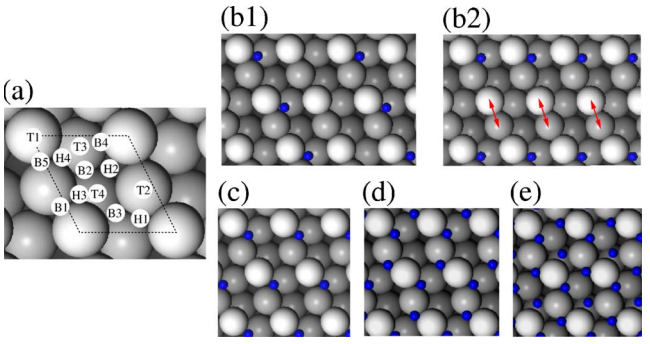

FIG. 5. (Color online) Top views of (a) Re(11$\bar{2}$1) showing all binding sites at which N adsorption has been studied as well as the most stable structures of nitrogen-covered Re(11$\bar{2}$1) with different overlayers and coverages: (b1) (1×2)-1N and (b2) (2×1)-1N overlayer at 0.5 GML, (c) (1×1)-1N overlayer at 1.0 GML, (d) (1×1)-2N overlayer at 2.0 GML, (e) (1×1)-3N overlayer at 3.0 GML. The arrows in structure (b2) indicate the Re atoms that move toward each other upon relaxation (row-pairing effect).

D. Nitrogen adsorption on Re surfaces

1. N/Re(11$\bar{2}$1)

Re(11$\bar{2}$1) is the substrate orientation onto which faceting occurs after adsorption of nitrogen. Therefore, before investigating the faces of the experimentally observed Re(13$\bar{4}$2) facets, we will discuss the adsorption of nitrogen on Re(11$\bar{2}$1). This will also allow us to clearly compare the changes in surface stability introduced by the adsorbates that finally lead to the observed morphology changes.

Figure 5(a) displays 13 probable binding sites that were considered in the present work. In the following we will use geometrical coverages (GMLs), which are defined as the number of adsorbed N atoms per corresponding (1×1) unit cell [dashed box in Fig. 5(a)]. We studied the adsorption of atomic nitrogen for coverages of 0.5 GML, having either (1×2) or (2×1) periodicity, as well as 1.0, 2.0, and 3.0 GML with (1×1) periodicity. Figure 5 presents the most stable configurations, for which the binding energies are summarized in Table IV. All adsorption energies reported here are referenced to half a N_2 molecule.

The most favorable adsorption site for N at 0.5 and 1.0 GML is the H4 site, where adsorbates bind to one top layer, the nearby second layer, and a third-layer Re atom finally resulting in a threefold binding. Our calculations reveal that for 0.5 GML [Fig. 5(b2)] the binding energy is 0.18 eV higher than with 1.0 GML [Fig. 5(c)]. This reduction in binding energy of N when going from 0.5 to 1.0 GML cannot solely related to N—N repulsion because: (1) even at $\Theta=1.0$ GML there is still a distance of at least ~4.8 Å between adjacent N atoms; (2) the binding energy of N with (1×1)-1N is very similar to that with (1×2)-1N overlayer; and (3) recent calculations have shown that the repulsive interactions between even more electronegative adatoms (i.e., oxygen) at $\Theta=1.0$ GML are negligible.[28]

TABLE IV. Binding energies (referenced to $\frac{1}{2}$ N_2) for nitrogen on Re(11$\bar{2}$1) at different coverages; only the most stable structure for each coverage is listed.

Coverage (GML)		E_{bind} (eV)
0.5	Figure 5(b1)	1.68
	Figure 5(b2)	1.83
1.0		1.66
2.0		1.21
3.0		0.81

After comparing the geometry of (1×1), (2×1), and (1×2)-1N with that of the clean surface, an interesting effect could be observed. In the (2×1)-1N structure, Re atoms on the zigzaglike ridges [connected by arrows in Fig. 5(b2)], which are not bound to the adatom, reduce their interatomic distance significantly by ~0.13 Å. This behavior, which has also been observed for Re(10$\bar{1}$0), Re(10$\bar{1}$1), Ir(311), and Ir(110) surfaces and which seems to be more general for the 5*d* elements, is known as *row pairing*.[28] Lower binding energies are obtained on Re(11$\bar{2}$1) for the (1×1)-1N and (1×2)-1N adlayers, structures for which row pairing is absent.

We used the calculated binding energies of nitrogen for 1.0 GML at the various surface sites together with a cubic spline interpolation to construct the full potential-energy surface (PES). The PES allows us to gain qualitative insights into the trends of adsorbate diffusion. The PES in Fig. 6 shows that the largest energy barrier for diffusion along the –H4–B3–B5–H4–direction [path (a)] is ~0.8 eV, which is comparable to the energy barrier of 0.9 eV we have obtained for the lower-indexed Re(10$\bar{1}$0) surface. In addition, diffusion of nitrogen along the zigzag rows [path (b)] is hindered by a very high barrier of ~1.6 eV.

At 2.0 GML, H4 sites are still preferred, while the second atom binds at threefold H1 sites [see Fig. 5(d)]. Increasing the nitrogen coverage to 3.0 GML, we find the most stable structure [Fig. 5(e)] to be similar to the one obtained for 2.0 GML with the third N atom at T4.

We will briefly discuss the binding energies versus coverages for N/Re(11$\bar{2}$1). As Fig. 7 shows, at 1.0 GML there is an absolute adsorption energy decrease compared to 0.5 GML, which most probably originates from the absence of row-pairing effects as discussed above. Clearly a decrease in the binding energy is also observed for N in the range of $1.0\leq\Theta\leq3.0$ GML, which is due to N—N repulsion and the occupation of less stable binding sites (in addition to the most stable H4 site). The second and third N atoms prefer largest separation from the already adsorbed N atoms. Adsorption sites that satisfy this requirement are H1 at 2.0 GML as well as H1 and T4 at 3.0 GML. We obtained the averaged energy for binding a single nitrogen per unit cell $\bar{E}_{bind}$ and estimated the N—N interaction by evaluating the following difference:

$$\Delta E_{int}=\bar{E}_{bind}-E_{bind}. \quad (13)$$

For 2.0 GML, we found $\Delta E_{int}=1.53-1.21=0.32$ eV, which means a relatively strong N—N repulsion. The binding en-

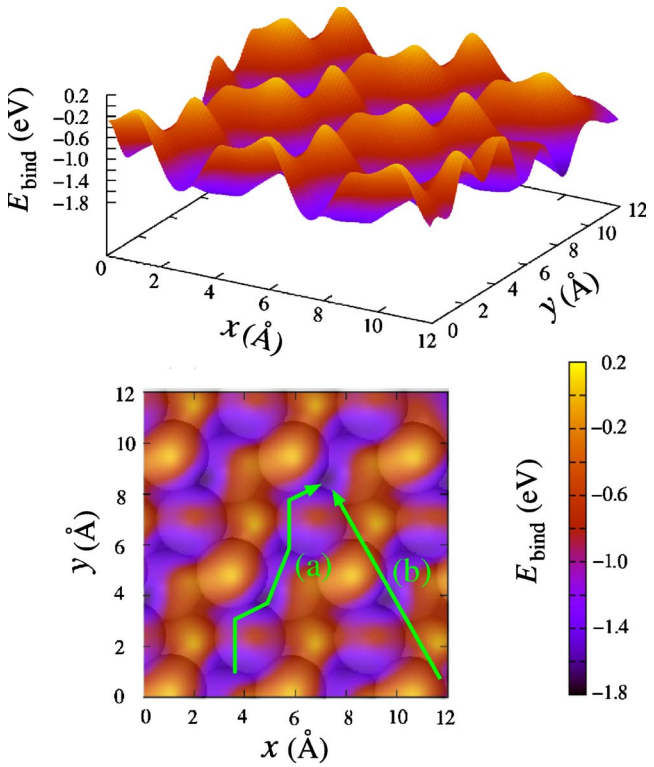

FIG. 6. (Color online) Adsorption energy distribution (referenced to $\frac{1}{2}N_2$) for binding 1.0 GML of atomic nitrogen onto Re(11$\bar{2}$1). The arrows indicate different paths for N diffusion on the surface.

ergy is even further lowered at 3.0 GML, since in order to reduce the strong interaction between adsorbates the third N atom per unit cell binds at site T4, which was an unstable site for N at lower coverages. While these coverages might not be stabilized by nitrogen exposure, for the O-Pd(111) system Seitsonen *et al.*[36] have shown that the accessibility for this N coverage can be realized by using differential heat of adsorptions.

2. N/Re(13$\bar{4}$2)

Experimentally, it was found that nitrogen adsorption causes the Re(11$\bar{2}$1) surface to become completely faceted,

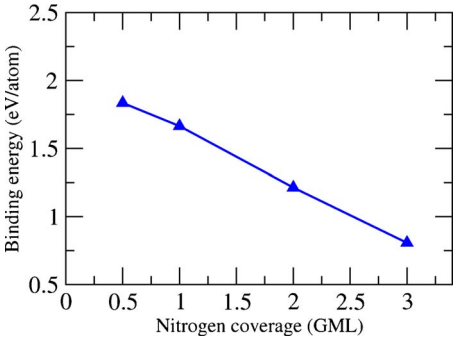

FIG. 7. (Color online) Binding energy (referenced to $\frac{1}{2}N_2$) as a function of nitrogen coverage on Re(11$\bar{2}$1).

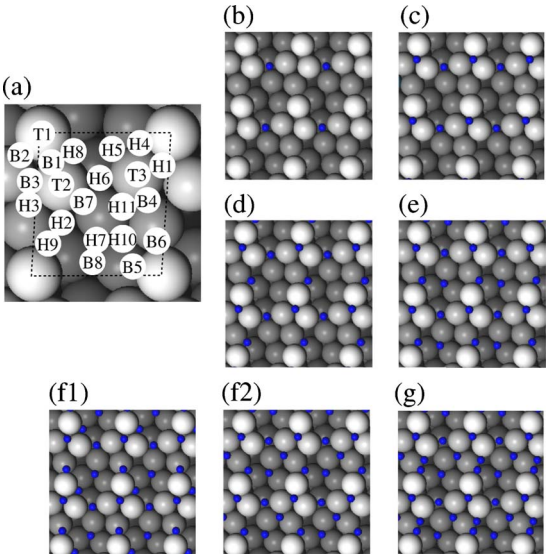

FIG. 8. (Color online) Top views of (a) Re(13$\bar{4}$2) showing all binding sites at which N adsorption has been studied as well as the most stable structures of nitrogen-covered Re(13$\bar{4}$2) at different coverages: (b) 1.0 GML, (c) 2.0 GML, (d) 3.0 GML, (e) 4.0 GML, (f1) and (f2) 5.0 GML, and (g) 6.0 GML.

forming two-sided ridgelike structures. The orientations of the faces that are exposed by the nanoridges are Re(13$\bar{4}$2) and Re(31$\bar{4}$2). Since both surface orientations are equivalent, in the following we will investigate the adsorption of atomic nitrogen on Re(13$\bar{4}$2) for coverages ranging from 1.0 to 6.0 GML, which are almost comparable adsorbate densities as used on Re(11$\bar{2}$1) with coverages ranging from 1.0 to 3.0 GML.

Figure 8(a) shows 21 probable adsorption sites, which we assumed as initial positions for N adsorption. Our results are summarized in Figs. 8(b)–8(g) and Table V.

It turned out that 1.0 GML nitrogen prefers the H6 position [Fig. 8(b)], where each adsorbate forms bonds to second-, third-, fifth-, and eighth-layer Re atoms, finally resulting in a fourfold binding. The calculated adsorption energy is higher than that obtained for Re(11$\bar{2}$1).[28] As mentioned in Sec. III B 2, Re(13$\bar{4}$2) is vicinal to the (01$\bar{1}$1)

TABLE V. Binding energies (referenced to $\frac{1}{2}N_2$) for nitrogen on Re(13$\bar{4}$2) at different coverages; only the most stable structure for each coverage is listed (see Fig. 8).

Coverage (GML)		E_{bind} (eV)
1		2.35
2		2.20
3		1.89
4		1.54
5	Figure 8(f1)	1.22
	Figure 8(f2)	1.20
6		0.95

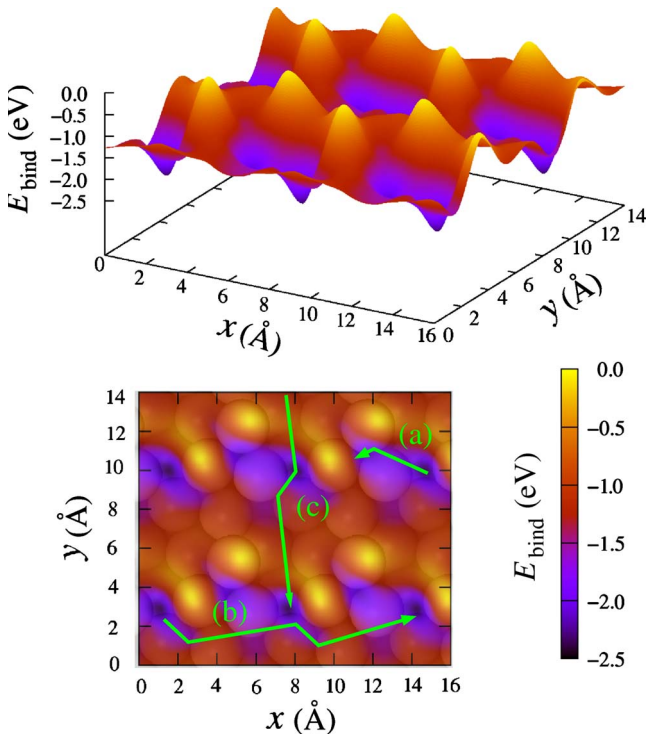

FIG. 9. (Color online) Adsorption energy distribution (referenced to $\frac{1}{2}N_2$) for binding 1.0 GML of atomic nitrogen onto Re(13$\bar{4}$2). The arrows indicate different paths for N diffusion on the surface.

surface with kinked steps and close-packed (01$\bar{1}$1) terraces.[17] In comparison, binding low amounts of nitrogen on Re(01$\bar{1}$1) has a 0.14 eV lower adsorption energy than binding on Re(13$\bar{4}$2). This shows that N binding to the adsorption sites between the (01$\bar{1}$1) terraces is more favorable than that on the (01$\bar{1}$1) terraces.

The PES (Fig. 9) shows that N diffusion from H6 to H1 or B1 sites [path (a)] has a barrier of ~0.5 eV. All other adsorption positions that have been considered are significantly less stable than binding to H6, H1, and B1 sites, leading to high diffusion barriers along paths (b) and (c) of ~1.5 eV. Therefore, N atoms would be trapped in H6 sites at low temperatures while they may also occupy H1 and B1 sites at higher temperatures.

At 2.0 GML and above, N atoms start occupying sites on the (01$\bar{1}$1) terraces [see Figs. 8(c)–8(g)]. Interestingly, even two and three nitrogen atoms per unit cell give a low adsorbate density and therefore only minor N—N repulsion is found at these coverages. At 2.0 GML, the calculated binding energy of 2.20 eV is only 0.01 eV lower than the corresponding $\bar{E}_{bind}$ value. For 3.0 GML, the binding energy of 1.89 eV is again very close to the value of 1.88 eV obtained for $\bar{E}_{bind}$. Interactions between adsorbates start to become significant at $\Theta=4.0$ GML and higher. Consequently, at 4.0 GML the binding energy of the most stable configuration is 0.14 eV lower than $\bar{E}_{bind}=1.68$ eV. The preferred configuration for 5.0 GML with a binding energy of 1.22 eV ($\bar{E}_{bind}=1.49$ eV) shows an increasing N—N repulsion. Finally, at a coverage of 6.0 GML, a notable difference is obtained between $E_{bind}=0.95$ eV and $\bar{E}_{bind}=1.63$ eV.

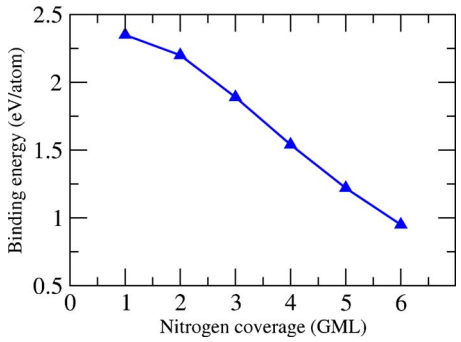

FIG. 10. (Color online) Binding energy (referenced to $\frac{1}{2}N_2$) as a function of nitrogen coverage on Re(13$\bar{4}$2).

From Fig. 10 it can be clearly seen that the binding energy decreases with increasing N coverage. As discussed above, this decrease is low for $\Theta \leq 2.0$ GML, but becomes rapid at higher nitrogen coverages. This trend follows the preference in binding sites. At 2.0 GML, besides already occupied H6 sites, the second N atom per unit cell populates the H1 site, which is only 0.28 eV less stable than binding at H6, while at $\Theta \geq 3.0$ GML the additional N adsorbates have to occupy the remaining vacant positions that are considerably less favored. Since the interaction between nitrogen adatoms for $\Theta=2.0$ and 3.0 GML is very weak, the reduction in binding energy for the low coverages is only due to the energy difference between different occupied sites.

The resulting atom density of 2.0 GML of N on Re(13$\bar{4}$2) is comparable to 1.0 GML on Re(11$\bar{2}$1) since the surface area per (1×1) unit cell of the former surface is almost twice as large as of the latter one (see Table III). A comparison between Figs. 7 and 10 shows that for all studied coverages the binding energy on Re(13$\bar{4}$2) is much higher than that on Re(11$\bar{2}$1). This might qualitatively support the stabilization of Re(13$\bar{4}$2) facets on the Re(11$\bar{2}$1) substrate after adsorption of N. However, for a quantitative understanding we still need to calculate the surface free energies of relevant surfaces to compare the stability of initial and final structures. This will be the subject of Sec. IV.

3. *Density of states of* N/Re(11$\bar{2}$1) *and* N/Re(13$\bar{4}$2)

Now, we will briefly compare in simple terms the binding of N on the Re(11$\bar{2}$1) and Re(13$\bar{4}$2) surfaces. For this purpose we analyzed adsorbate-induced changes in the surface density of states (ΔDOS), which is the difference between the density of states of the clean and N-covered surface

$$\Delta\mathrm{DOS} = \mathrm{DOS}(\mathrm{Re}_{5d} + \mathrm{N}_{2p}) - \mathrm{DOS}(\mathrm{Re}_{5d}). \quad (14)$$

Figure 11 shows the projected DOS of selected Re surface atoms' *d* bands as well as the adsorbate-induced changes, ΔDOS, on the total DOS. We have chosen the structures with 1.0 GML of N in which the adsorbate—adsorbate interactions are comparably small. Due to changes in the bonding

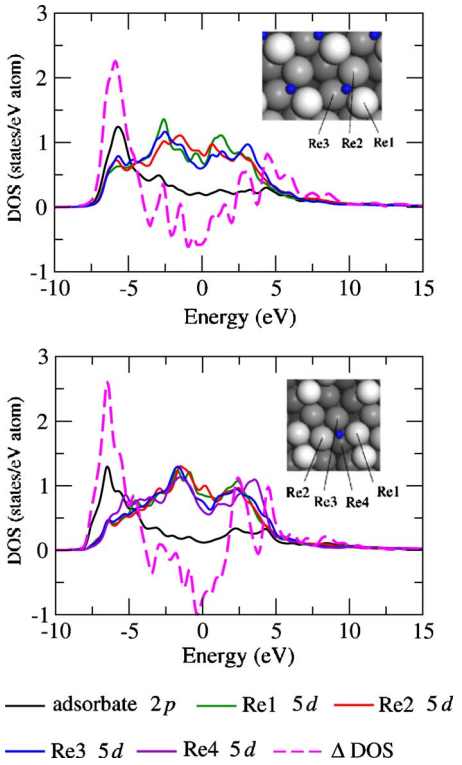

FIG. 11. (Color online) ΔDOS and PDOS for N/Re(11$\bar{2}$1) (top) and N/Re(13$\bar{4}$2) (bottom). The energy zero shows the Fermi level.

states both surfaces have a large peak in the ΔDOS curve between −7 and −5 eV. The other, somewhat smaller peaks in the ΔDOS, positioned above the Fermi energy, seem to be due to the antibonding states. Comparing both surfaces, the bonding level for Re(13$\bar{4}$2) is lower in energy than the corresponding ΔDOS peak of Re(11$\bar{2}$1). In addition, on the latter surface we observe a small accumulation peak at around −3.2 eV, where there is an overlap between Re 5*d* and N 2*p* states, probably being attributed to the occupation of antibonding states. This behavior is in agreement with the calculated adsorption energies discussed in the previous section, where we obtained stronger interaction of N with Re(13$\bar{4}$2) compared to Re(11$\bar{2}$1).

IV. SURFACE PHASE DIAGRAM OF N/Re(11$\bar{2}$1)

The surface free energy for the faceted surface was calculated using the left side of Eq. (11) with the parameters for the partial surface areas and facet tilt angles summarized in Table III. Each term of this equation was evaluated by using Eq. (2) together with the DFT-calculated total energies discussed in the previous sections.

Figure 12 shows the surface phase diagram including clean and nitrogen-covered surfaces of: (1) the flat Re(11$\bar{2}$1) substrate and (2) two-sided ridgelike structures with (13$\bar{4}$2) and (31$\bar{4}$2) faces. Prior to discussing the results for N/Re(11$\bar{2}$1), we should mention that experimentally N was deposited on Re(11$\bar{2}$1) using gaseous NH_3, whereas our

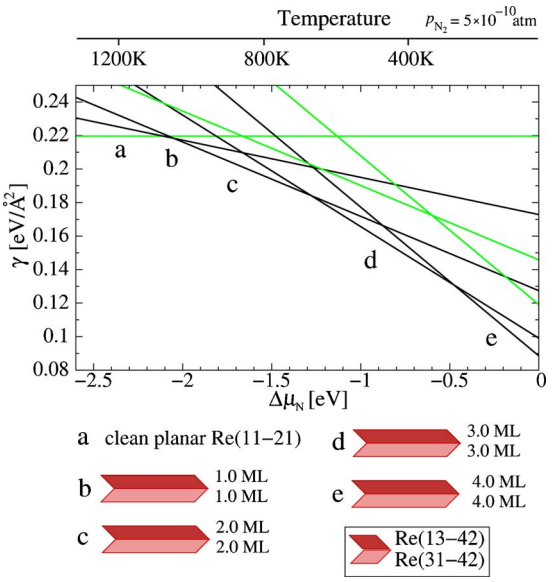

FIG. 12. (Color online) Surface phase diagram for N-induced faceting of planar Re(11$\bar{2}$1) showing the surface free energy as function of the nitrogen chemical potential referenced as $\Delta\mu_N = \mu_N - \frac{1}{2}E^{tot}_{N_2}$.

phase diagram is based on adsorption of nitrogen from N_2. The assumption of a thermodynamic equilibrium with a N_2 atmosphere is justified by the fact that all nitrogen atoms desorbing from the Re surfaces combine to N_2.

The surface phase diagram (Fig. 12) shows that, at nitrogen partial pressures of $p_{N_2}=5\times10^{-10}$ atm and $T \geq 1080$ K, no nitrogen is adsorbed on the surface. This temperature is in agreement with the experimental value of 1100 K for desorption of nitrogen from the surface, which according to our calculations should be planar Re(11$\bar{2}$1). Clean facets of two-sided ridges (see Sec. III C) are less stable by 5 meV/Å^2. As soon as nitrogen adsorbs below 1080 K, the experimentally observed nanofacets of two-sided ridges, combining Re(13$\bar{4}$2) and Re(31$\bar{4}$2) faces, become the thermodynamically preferred surface phases (phases b–e). Over the whole temperature range of $T<1080$ K these nanofacets (envelope lines in the phase diagram) are significantly more stable than nitrogen-covered planar Re(11$\bar{2}$1) (higher-lying lines).

As mentioned in Sec. III D 1, we used GMLs, which are the number of adsorbed nitrogen atoms per (1×1) unit cell. In comparison, experiments usually use physical coverages (PMLs), in which surface saturation is defined to be 1 ML. Unfortunately, there are no direct measurements of the saturation coverage of N on Re(11$\bar{2}$1). However, by using the highest possible nitrogen coverage phases from our phase diagram to define saturation coverage, we obtain an adsorbate density on Re(11$\bar{2}$1) of 0.89×10^{15} atoms/cm^{-2} for nitrogen. This leads to the following approximate conversion between GML and PML for the Re(11$\bar{2}$1) substrate: 2.0 GML-N ≡ 1.0 PML-N. Experimental observations proposed that the facets start to form when the nitrogen coverage is larger than 0.4–0.5 PML at 5×10^{-10} atm and tem-

peratures above 700 K. Under these conditions our phase diagram shows phase c, which has 2.0 GML of nitrogen on each face, to be thermodynamically stable. Projecting this coverage onto the Re(11$\bar{2}$1) substrate would lead to around 1.0 GML, which converts to 0.5 PML, being in good agreement with the experimental value. Lowering the temperature (at fixed pressure) does not cause the surface morphology to change but leads to an increase in the nitrogen coverage on the ridges.

When a metal surface is in contact with a nitrogen atmosphere, bulk nitride might form under specific temperature and pressure conditions. Thermodynamically, a bulk nitride Re_xN_y is stabilized when the nitrogen chemical potential $\Delta\mu_N$ is larger than $\Delta H_f/y$, where ΔH_f is the heat of formation of the corresponding bulk nitride. There is experimental evidence that a stable Re nitride cannot be obtained directly from the elements.[37] Therefore, although at lower temperatures one would expect a bulk Re nitride to become thermodynamically stable, such a stable compound has not been observed.

In order to investigate the sensitivity of our results on choosing a different xc functional, we additionally calculated the most relevant surface structures with the LDA functional and generated the equivalent surface phase diagram. Figure 13 shows the stability range of different phases with respect to temperature and pressure evaluated using the PBE and LDA functional. We find that the overall phase ordering and therefore the conclusions drawn above remain unchanged when using LDA.

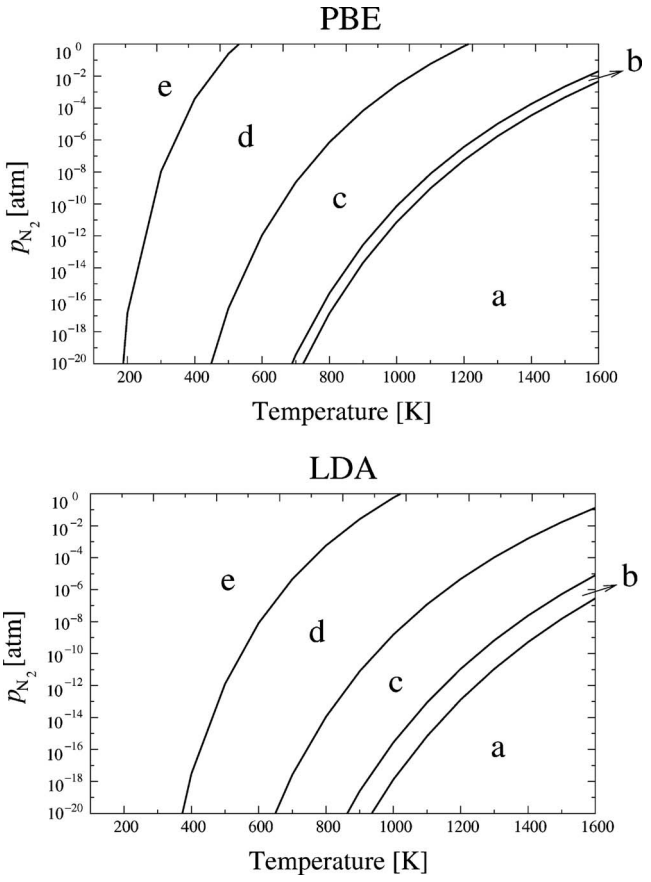

FIG. 13. Surface phase diagrams for Re(11$\bar{2}$1) in contact with a N_2 atmosphere comparing the PBE and LDA exchange-correlation functionals. Labels correspond to the surface phases as indicated in Fig. 12.

V. CONCLUSION

In this paper we have studied clean and nitrogen-covered surfaces of Re(11$\bar{2}$1) and Re(13$\bar{4}$2) to provide detailed information on the geometric and electronic structure. Performing extensive DFT calculations, it has been shown that binding of N to Re(13$\bar{4}$2) is much stronger than compared to the more close-packed Re(11$\bar{2}$1) surface. This is due to the specific surface structure of Re(13$\bar{4}$2) allowing strongly interacting adsorbates to occupy rather specific binding sites being located between the (10$\bar{1}$1) terraces. Using the obtained energetics in conjunction with thermodynamic considerations, we found that N/Re(13$\bar{4}$2) is considerably more stable than N/Re(11$\bar{2}$1), even leading to surface faceting over the whole range of N coverages considered in this work. Our work indicates that it is possible to stabilize facets of rough faces on initially more close-packed substrates in the presence of certain gases. This might have interesting implications for understanding the surface morphology and performance of Re-based catalysts that are operated under nitrogen-rich conditions.

ACKNOWLEDGMENTS

The authors gratefully acknowledge support from the "Deutsche Forschungsgemeinschaft" (DFG) as well as by the bw-grid for computing resources (Ref. 38). Further, support by the European Union through the Marie-Curie Initial Training Network ELCAT, Proposals No. 214936-2 and No. 2008-2012, is acknowledged.

*timo.jacob@uni-ulm.de; http://www.echem.uni-ulm.de

[1] S. G. Sun and J. Clavilier, Chem. J. Chin. Univ. **11**, 998 (1990).
[2] W. Chen, T. E. Madey, A. L. Stottlemyer, J. G. G. Chen, P. Kaghazchi, and T. Jacob, J. Phys. Chem. C **112**, 19113 (2008).
[3] N. Hoshi, S. Kawatani, M. Kudo, and Y. Hori, J. Electroanal. Chem. **467**, 67 (1999).
[4] W. F. Banholzer and R. I. Wasel, J. Catal. **85**, 127 (1984).
[5] J. G. Wang, W. X. Li, M. Borg, J. Gustafson, A. Mikkelsen, T. M. Pedersen, E. Lundgren, J. Weissenrieder, J. Klikovits, M. Schmid, B. Hammer, and J. N. Andersen, Phys. Rev. Lett. **95**, 256102 (2005).
[6] I. E. Wachs, G. Deo, A. Andreini, M. A. Vuurman, and M. de

Boer, J. Catal. **160**, 322 (1996).
[7] Y. Z. Yuan, T. Shido, and Y. Iwasawa, Chem. Comm. **15**, 1421 (2000).
[8] J. Liu, E. Zhan, W. Cai, J. Li, and W. Shen, Catal. Lett. **120**, 274 (2008).
[9] M. E. Bussell, A. J. Gellman, and G. A. Somorjai, J. Catal. **110**, 423 (1988).
[10] M. Asscher, J. Carrazza, M. M. Khan, K. B. Lewis, and G. A. Somorjai, J. Catal. **98**, 277 (1986).
[11] R. Kojima, H. Enomoto, M. Muhler, and K. Aika, Appl. Catal., A **246**, 311 (2003).
[12] R. Döll, L. Hammer, K. Heinz, K. Bedürftig, U. Muschiol, K. Christmann, A. P. Seitsonen, H. Bludau, and H. Over, J. Chem. Phys. **108**, 8671 (1998).
[13] J. Lenz, P. Rech, K. Christmann, M. Neuber, C. Zubragel, and E. Schwarz, Surf. Sci. **269-270**, 410 (1992).
[14] C. Pauls, C. D. Przyrembel, and K. Christmann, J. Phys. Chem. B **108**, 14749 (2004).
[15] D. M. Zehner and H. E. Farnsworth, Surf. Sci. **30**, 335 (1972).
[16] J. W. He and D. W. Goodman, J. Phys. Chem. **94**, 1502 (1990).
[17] H. Wang, Ph.D. thesis, Rutgers University, 2008.
[18] J. Gustafson, A. Resta, A. Mikkelsen, R. Westerström, J. N. Andersen, E. Lundgren, J. Weissenrieder, M. Schmid, P. Varga, N. Kasper, X. Torrelles, S. Ferrer, F. Mittendorfer, and G. Kresse, Phys. Rev. B **74**, 035401 (2006).
[19] R. Westerström, J. Gustafson, A. Resta, A. Mikkelsen, J. N. Andersen, E. Lundgren, N. Seriani, F. Mittendorfer, M. Schmid, J. Klikovits, P. Varga, M. D. Ackermann, J. W. M. Frenken, N. Kasper, and A. Stierle, Phys. Rev. B **76**, 155410 (2007).
[20] T. E. Madey, W. Chen, H. Wang, P. Kaghazchi, and T. Jacob, Chem. Soc. Rev. **37**, 2310 (2008).
[21] E. Kaxiras, Y. Bar-Yam, J. D. Joannopoulos, and K. C. Pandey, Phys. Rev. B **35**, 9625 (1987).
[22] M. Scheffler, *Physics of Solid Surfaces* (Elsevier, Amsterdam, 1987).
[23] G.-X. Qian, R. M. Martin, and D. J. Chadi, Phys. Rev. B **38**, 7649 (1988).
[24] K. Reuter and M. Scheffler, Phys. Rev. B **65**, 035406 (2001).
[25] M. D. Segall, P. L. D. Lindan, M. J. Probert, C. J. Pickard, P. J. Hasnip, S. J. Clark, and M. C. Payne, J. Phys.: Condens. Matter **14**, 2717 (2002).
[26] D. Vanderbilt, Phys. Rev. B **41**, 7892 (1990).
[27] P. Kaghazchi and T. Jacob, Phys. Rev. B **81**, 075431 (2010).
[28] P. Kaghazchi, Ph.D. thesis, Freie University Berlin, 2009.
[29] J. P. Perdew, K. Burke, and M. Ernzerhof, Phys. Rev. Lett. **77**, 3865 (1996).
[30] B. G. Pfrommer, M. Cote, S. G. Louie, and M. L. Cohen, J. Comput. Phys. **131**, 233 (1997).
[31] D. R. Stull and H. Prophet, *JANAF Thermochemical Tables*, 2nd ed. (U.S. National bureau of Standards, Washington, DC, 1971).
[32] C. Herring, Phys. Rev. **82**, 87 (1951).
[33] C. Kittel, *Introduction to Solid State Physics* (Wiley, New York, 1996).
[34] H. L. Davis and D. M. Zehner, J. Vac. Sci. Technol. **17**, 190 (1980).
[35] H. Wang (private communication).
[36] A. P. Seitsonen, Y. D. Kim, S. Schwegmann, and H. Over, Surf. Sci. **468**, 176 (2000).
[37] P. Clark, B. Dhandapani, and S. Oyama, Appl. Catal., A **184**, 175 (1999).
[38] bwGRiD, http://www.bw-grid.de, member of the German D-Grid initiative, funded by the Ministry for Education and Research (Bundesministerium für Bildung und Forschung) and the Ministry for Science, Research and Arts Baden-Württemberg (Ministerium fuer Wissenschaft, Forschung und Kunst Baden-Württemberg).